A mechanism for growth of topological entropy

Daniel Wilczak*,[1] Sergio Serrano,[2] and Roberto Barrio[3]
[1)] *Faculty of Mathematics and Computer Science. Jagiellonian University. Łojasiewicza 6, 30-348 Kraków, Poland.*
[2)] *Departamento de Matemática Aplicada and IUMA. University of Zaragoza. E-50009. Spain. CODY. University of Zaragoza. E-50009. Spain.*
[3)] *Departamento de Matemática Aplicada and IUMA. University of Zaragoza. E-50009. Spain. CODY. University of Zaragoza. E-50009. Spain.*

(*Electronic mail: rbarrio@unizar.es)

(*Electronic mail: sserrano@unizar.es)

(*Electronic mail: Daniel.Wilczak@uj.edu.pl)

(Dated: 21 September 2025)

The theoretical and numerical understanding of the key concept of topological entropy is an important problem in dynamical systems. While most existing studies focus on discrete-time systems (maps), this work examines a continuous-time scenario involving global changes in the structure of an observed attractor. As a representative example, we consider the classical Rössler system. For a specific range of parameters of the system, we prove the existence of a trapping region for certain Poincaré map, which contains a nonempty, compact and connected invariant set on which the topological entropy of the Poincaré map is positive. Additionally, we prove the existence of a sequence of periodic orbit bifurcations that lead to an increase in the topological entropy of this Poincaré map. Our results further reveal that the topological structure of the maximal invariant set in the trapping region evolves as the parameters of the system vary. These findings are rigorously supported by computer-assisted proofs, employing interval arithmetic techniques to compute guaranteed bounds on the Poincaré map and its derivatives.

There are different definitions of an attractor (see Milnor [1] for an overview) but a common required geometric property is that it is a compact forward invariant set that attracts nearby trajectories. Therefore, attractors are usually easily identifiable objects in numerical simulations of dynamical systems. Understanding their internal dynamics is usually a challenging task. An attractor may contain proper invariant subsets, such as subattractors, hyperbolic chaotic invariant sets or even attracting cycles. Stable periodic orbits of very high period might be difficult to detected when they coexists with a chaotic invariant set[2,3]. Conversely, various chaos indicators, such as topological entropy and Lyapunov exponents, provide quantitative insights into the complexity of a system's dynamics. Notably, Lyapunov exponents can also serve to differentiate between chaotic and hyperchaotic behavior[4].

The aim of this paper is twofold. Firstly, we present a simple model — a univariate map — in which the topological entropy grows to infinity as the parameter of the map increases. A sequence of saddle-node bifurcations leads to the coexistence of a stable fixed point and a chaotic invariant set, for which the topological entropy is finite, yet potentially very large. Second, we study a continuous-time model: the Rössler system[5]. We prove that, for an explicit range of its parameters, there is a trapping region for a specific Poincaré map. This trapping region contains a compact and connected maximal invariant set. This invariant set certainly contains an attractor of the system. Further analysis of the Poincaré shows that certain quantity, which reflects the number of folds in the image of the trapping region by the Poincaré map, varies with the parameter. Consequently, the topological structure of the maximal invariant set also changes with the parameter. Finally, we illustrate that this Poincaré map exhibits a scenario of entropy growth similar to that observed in the model map.

I. INTRODUCTION.

The concept of topological entropy, one of the most important topological invariants, was first introduced by Adler, Konheim and McAndrew[6] and later adopted to continuous maps on compact metric spaces by Dinaburg[7] and Bowen[8]. It measures the complexity of dynamics generated by a continuous map $f : X \to X$ defined on a compact metric space (X,d). A subset $E \subset X$ is called (n,ε)-separated if

$$\inf\left\{\max_{0\le i<n} d(f^i(x),f^i(y)) : x,y\in E, x\neq y\right\} \ge \varepsilon.$$

The entropy of f with respect to metric d is defined as

$$h_d(f) = \lim_{\varepsilon\to 0}\left(\limsup_{n\to\infty}\frac{1}{n}\log N_d(f,n,\varepsilon)\right),$$

where $N_d(f,n,\varepsilon)$ is the maximum cardinality of an (n,ε)-separated set. Thus, the entropy measures the exponential growth rate of the number of points in X with distinguishable segments of orbits of length n up to resolution ε.

It can be shown that if d' is another metric on X that defines the same topology as d, then $h_d(f) = h_{d'}(f)$. Therefore, this is simply denoted by $h_{\text{top}}(f)$ and is known as the topological entropy of f. For a more comprehensive description we refer the reader to the book by Katok and Hasselblatt[9].

Changes in topological entropy with respect to the parameter of the system indicate bifurcations, which affect the global structure of orbits. As Milnor[10] points out, it is natural to ask whether topological entropy can be calculated efficiently. Although it is usually impossible to compute the entropy exactly[10,11], it can often be bounded from below by proving (semi)conjugacy to shift dynamics, for example. Clearly, there are many open questions in the study of dynamical systems, one of them being the efficient computation of topological entropy for higher-dimensional maps.

Another important concept used in this article is an attractor. Although there are several different definitions of an attractor, we will use that proposed by Milnor[1]. Let M be a compact manifold with boundary or not. A compact subset $A \subset M$ is called an attractor for a continuous map or semi flow on M if

- the basin of attraction $\rho(A) = \{x \in M : \omega(x) \subset A\}$ has positive measure (here by $\omega(x)$ we denote the ω-limit set) and
- if $A' \subset A$ and $\rho(A) \setminus \rho(A')$ is of zero-measure then $A = A'$.

In the above definition one can choose an arbitrary measure which is equivalent to the Lebesgue measure when restricted to any coordinate neighborhood.

The aim of this paper is to present an algorithmic approach to demonstrate the existence of global changes in the topological structure of invariant sets in continuous-time systems as a parameter of the system varies. As a paradigmatic example, we consider the Rössler system[5]

$$\dot{x} = -(y+z), \qquad \dot{y} = x + ay, \qquad \dot{z} = b + z(x-c). \tag{1}$$

This model has been extensively studied in the literature[5,12–16], showing different types of observed attractors.

We fix the parameters $b = 0.2$ and $c = 15$ of (1) and we analyse the system for an explicit range

$$a \in \mathscr{A} = [a_{\min}, a_{\max}] := [0.12, 0.3659]. \tag{2}$$

We will prove that, for $a \in \mathscr{A}$ there exists an explicit, compact trapping region for (1), which contains a maximal invariant set for (1). This maximal invariant set is either an attractor for the system or it contains an attractor. We will prove that this maximal invariant set undergoes bifurcations that lead to global changes in its topological structure. Although computing the exact value of the entropy for the Rössler system may be impossible, we will estimate the entropy of a certain Poincaré map of this system from below in different subintervals of the range $a \in \mathscr{A}$. We will also prove that, within the range $\mathscr{A}$ of parameters, there is a sequence of saddle-node bifurcations that gives rise to a semiconjugacy of the chosen Poincaré map to the Bernoulli shift on 2 up to 13 symbols, depending on the parameter range.

Providing paper-and-pencil proofs of the above type of results for a given model is rather impossible, except perhaps for very simple examples. Therefore, to consider the classical and seminal model (1), we will use the powerful machinery of so-called *validated numerics*[17–19].

Over the last few decades, efficient algorithms for validated integration of finite dimensional ODEs have been proposed[20–28]. Even if the explicit solutions to an ODE cannot be found exactly, it is often possible to compute bounds on the flow[25] or Poincaré maps[29] and their derivatives. These estimates can be used to verify whether the solutions satisfy carefully chosen inequalities, from which partial information about the underlying dynamics can be extracted. Computer-assisted techniques[30] are currently a very active field of research[4,31–38]. Rigorous numerical techniques can be applied to validate the existence of different phenomena observed in simulations, including the solution to the Smale's 14th problem[39] concerning the existence and non-uniform hyperbolicity of the Lorenz attractor.

The paper is organized as follows. Section II introduces a one-dimensional scenario that leads to the growth of topological entropy. Section III presents the results of biparametric numerical analysis of the Rössler system (1). Section IV provides the main results concerning the existence of a trapping region in the Rössler system and changes in the structure of its maximal invariant subset. These are Theorem 1, Theorem 2, Theorem 4 and Theorem 6. Section V contains computer-assisted proofs of the aforementioned main results.

II. TOY MODEL – THE SINE MAP

In order to present the geometry of the mechanism that leads to the growth of the entropy, let us consider the following one-dimensional toy model

$$f_a(x) = \frac{1}{2}\left(1 + \sin(a\pi x)\right), \qquad a \in \mathbb{R}. \tag{3}$$

Clearly, the interval $I = [0,1]$ is a forward invariant set for any parameter value $a \in \mathbb{R}$.

Figure 1 (plot (a)) shows the lower and upper bounds on the topological entropy (calculated using the algorithm by Góra and Boyarsky[40]) for the parameter range $a \in [0, 7.5]$. The upper bound is computed as $\frac{1}{k}\log_2 c_k$ for some large k, where c_k is the number of monotone slopes of f_a^k. We observe that, for larger values of the parameter a, the entropy grows like $\log_2 a$. In plot (b), we show the Lyapunov exponent of f_a for $a \in [0, 7.5]$. The plot indicates that regions with chaotic behavior are repeated at a distance of approximately 2 in the parameter a. Plot (c) provides the bifurcation diagram. We observe a sequence of saddle-node bifurcations that appear at a distance of around 2 in the parameter a, followed by period-doubling cascades leading to chaos, as shown by the Lyapunov exponent. On the bottom figure (d), we present the graph of the function map (3) for different parameter values of a. It is clear, that the number of monotone slopes of f_a in the domain $[0,1]$ is nondecreasing with the parameter a, passing from a unimodal to a multiple modal case. The thick lines denote the limit maps between n-modal and $n+1$-modal maps.

For the parameter value $a = 1/2$, function (3) is strictly monotone and thus the only limit sets are fixed points. At $a \approx 2.45855$, a saddle-node bifurcation occurs, creating a pair of stable and unstable fixed points – see Fig. 2. For

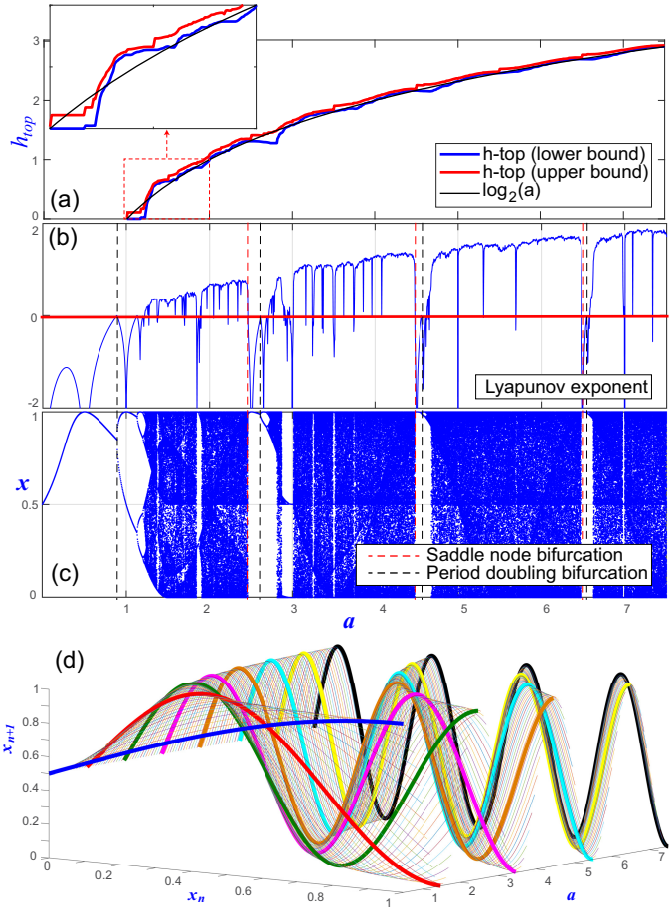

FIG. 1. (a) Lower and upper bounds on the topological entropy values of the sine model in the range $a \in [0, 7.5]$ and the value of $\log_2(a)$. (b) Lyapunov exponent of the map (3). (c) Bifurcation diagram. (d) 3D plot of the function map (3) depending on the parameter a.

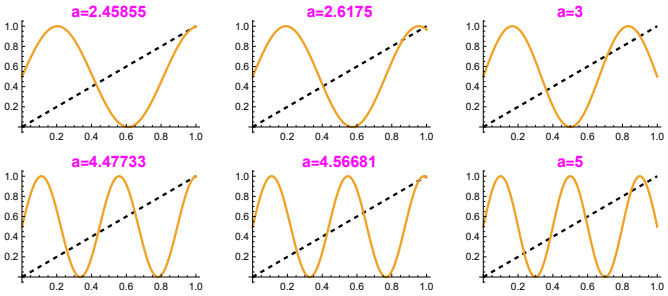

FIG. 2. Plot of $f_a(x)$ for different parameter values. A saddle-node bifurcation creates a pair of fixed points (left column). The stable fixed point then loses its stability via a period-doubling bifurcation (middle column). Further growth of the parameter leads to the creation of a new symbol for the conjugacy to symbolic dynamics (right column).

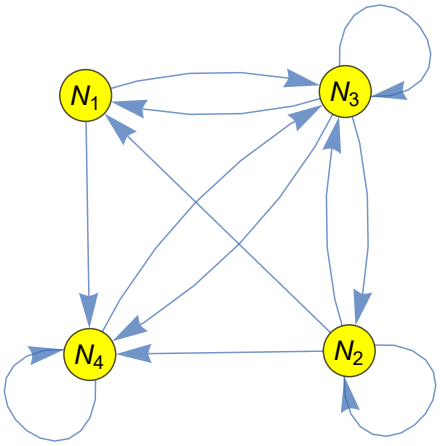

FIG. 3. Graph of symbolic dynamics of the sine model (3) for $a = 3$.

$a \approx 2.6175$, the stable fixed point loses its stability through a period-doubling bifurcation, which is the onset of chaotic dynamics via the well known cascade of period-doubling bifurcations. For $a = 3$, the interval $[0,1]$ can be split into subintervals $N_1 = [0, \frac{1}{6}]$, $N_2 = [\frac{1}{6}, \frac{1}{2}]$, $N_3 = [\frac{1}{2}, \frac{5}{6}]$ and $N_4 = [\frac{5}{6}, 1]$, in which the function is monotone. Every point $x \in N_1$ is mapped to either N_3 or N_4. The images of both N_2 and N_3 cover the range $[0,1]$. Finally, points $x \in N_4$ can be mapped to either N_3 or N_4. Note also that, for almost every $x \in [0,1]$, excluding a countable set of points $\mathscr{E} = \bigcup_{i\in\mathbb{N}} f_{a=3}^{-i}\left(\{0, \frac{1}{6}, \frac{1}{2}, \frac{5}{6}, 1\}\right)$, the trajectory $\{f_{a=3}^i(x)\}_{i\in\mathbb{N}}$ only visits the interiors of the N_i's, which are pairwise disjoint sets. For every $x \in \mathscr{I} := [0,1] \setminus \mathscr{E}$, the trajectory can be encoded as an infinite path on the directed graph shown in Fig. 3, that is a sequence of vertices $(c_i)_{i\in\mathbb{N}} \in \{1,2,3,4\}^{\mathbb{N}}$, such that $f_{a=3}^i(x) \in \text{int}N_{c_i}$ for $i \in \mathbb{N}$. This gives rise to a semiconjugacy between $f_{a=3}|_{\mathscr{I}}$ and the symbolic dynamics on four symbols. This notion will be introduced in Section IV.

Such scenario repeats when the parameter a is increasing. We observe a sequence of saddle-node bifurcations, which create a new pair of stable-unstable fixed points. In fact, when $a = (2n+1)/2$ for $n \in \mathbb{N}$, a new extremum of the map appears (see Fig. 2 (bottom)) and a new vertex can therefore be added to the graph of symbolic dynamics. Consequently, the topological entropy of f_a grows to infinity when $a \to \infty$.

We have briefly seen that interesting changes in the topological entropy happen in a simple case of the sine map. For instance, the celebrated article[41] proved that the entropy function is monotonically increasing for the quadratic (logistic) family. Therefore, a clear extension of this work, as well as an interesting open question, is to investigate what happens for continuous systems. In this direction, Section III presents the results of a biparametric numerical study of the Rössler system (1) exhibiting a similar mechanism of saddle-node bifurcations that may lead to growth of the entropy of the system. Then, in Section IV, we introduce an algorithmic method for constructing a computer-assisted proof of the existence of a trapping region for the Rössler system for an explicit range of parameter values, validating the existence of saddle-node bifurcations and computing a lower bound on the topological entropy of certain Poincaré map.

III. NUMERICAL STUDY OF THE RÖSSLER SYSTEM.

Unlike the sine model (3), the Rössler system (1) depends on three parameters. In this paper we fix the value of $b = 0.2$, but similar results could be obtained for other values (see Barrio, Blesa, and Serrano [12] for a more complete parametric study of the system). Figure 4 shows a biparametric plate in which the values of the parameters a and c vary. The plate shows the values of the first two Lyapunov exponents[42]. The colours (from green to red) represent the chaotic region, which is identified by the fact that the maximum Lyapunov exponent is greater than 0. A grey gradient represents the regular region (where a stable periodic orbit is observed), where the maximum exponent cancels out and the second Lyapunov exponent is represented. Black means that the second exponent is close to zero, and light grey represents a more stable periodic attractor. The white region on the right (with values of a close to 0.37) indicates that the dominant dynamics are the escape dynamics (see Barrio, Blesa, and Serrano [13] for a detailed explanation of the unbounded dynamics of the system). Several bifurcation curves obtained using the well-known continuation software AUTO[43,44] are superimposed on this plate. They are shown in blue for saddle-node bifurcations and in red for period-doubling bifurcations. This illustration is not exhaustive, but it is intended to show the huge number of bifurcations in the region shown. This results in a mixture of regions with different dynamics. To study the evolution of the model dynamics in more detail, we have selected a segment (with $c = 15$, marked in white and dashed grey) that crosses many of these regions and almost reaches the region of unbounded dynamics.

Let Π be a Poincaré section and $P : D \subset \Pi \to \Pi$ be the corresponding Poincaré map. For a fixed $p_0 \in D$ we set $p_n = P^n(p_0)$, $n > 0$ assuming the iterates exists. Let $\pi_x : D \to \mathbb{R}$ be a projection onto selected coordinate. We set $x_n = \pi_x(p_n)$, $n \geq 0$. The first return map (FRM) associated with the orbit of p_0 is defined as $\mathrm{FRM}(x_n) = x_{n+1}$. This formulation describes the discrete-time dynamical system induced by the continuous flow, projected onto a single coordinate axis, and captures the evolution of the system under successive returns to the section. As with the Rössler system (1), many dynamical systems used to model problems of a different nature are strongly dissipative[14,15,45–49]. Their dynamics are characterised by the contraction of their flow along the stable manifold of their equilibrium points being much greater than the expansion along the unstable manifold of their equilibrium points. For such strongly dissipative systems, the FRM provides a means of obtaining a qualitative description of the topology of invariant chaotic sets[46,50,51].

For our analysis, we define a Poincaré section

$$\Pi := \{(x,y,z) \in \mathbb{R}^3 : y = 0 \wedge \dot{y} = x < 0\}. \tag{4}$$

In the top part of Figure 5 long trajectory segments of (1) and the location of the Poincaré section (4) is shown. In the bottom part of Figure 5 plots of associated FRMs at both ends of the segment selected in Fig. 4. As can be seen, the structure of the second observed attractor (funnel type) is much more complex than that of the first (spiral type). This increase in complexity

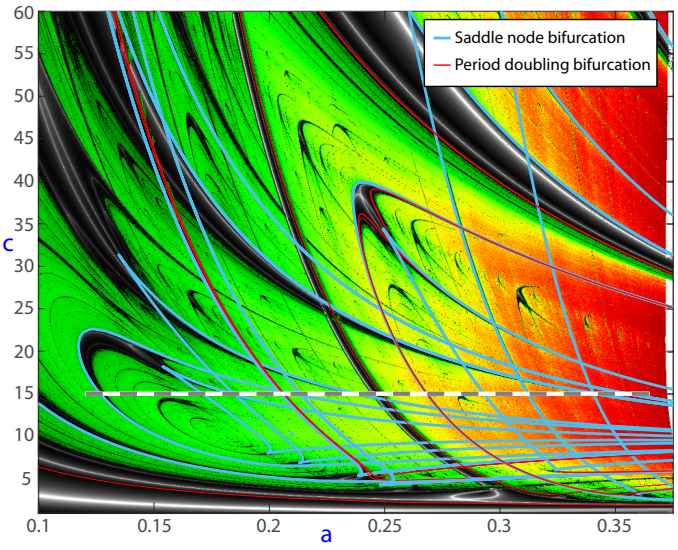

FIG. 4. Biparametric plot of the largest Lyapunov exponents of (1) with $b = 0.2$. Colour scale (from green to red) represents the chaotic regimes indicated by the maximum Lyapunov exponent. In black and white, regular dynamics (no chaos), where first exponent is null and the second is represented. Blue curves mark saddle-node bifurcations, while red curves indicate period-doubling bifurcations. The white and grey dashed segment marks the line (with $c = 15$) that will be studied in more detail in the rest of the paper.

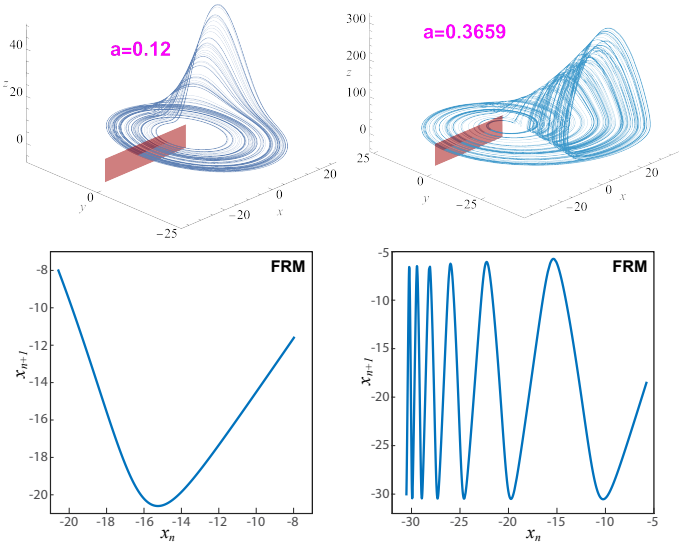

FIG. 5. Top: Poincaré section and a typical trajectory of (1) for $a = a_{\min} = 0.12$ (left) and $a = a_{\max} = 0.3659$ (right). Bottom: The corresponding FRM.

is reflected in a higher number of branches of the FRM. Figure 6 illustrates the FRM of the invariant set within a fine mesh of the chosen interval. This allows us to observe that the complexity of the set increases gradually. In this figure, we have used a thicker line to highlight some FRMs. They are approximately at the values of a where the change from n to $n+1$ branches occurs for n from 2 to 8. The following changes

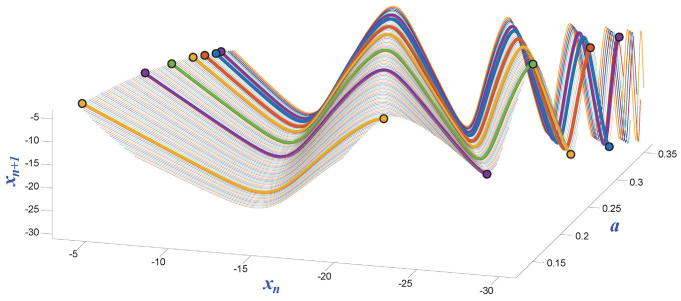

FIG. 6. FRMs for the existing invariant sets along the selected segment in Figure 4. The highlighted FRMs roughly indicate an increase in an additional branch.

appear closer together. Therefore, it would be necessary to use a finer mesh to mark them with sufficient precision. Note that our calculations of the FRM use chaotic invariant sets, whether they are attractors or not (i.e. whether they are saddle chaotic invariant sets). When the chaotic invariant set attracts all the dynamics around it, a good approximation of it, and therefore of its FRM, can be easily obtained. However, when a stable periodic orbit coexists with the chaotic invariant set, this is more difficult to achieve. Since the transition time near the invariant set is long, we can obtain a good approximation of it using Sprinkle method[52].

We can study the evolution of the dynamics along the selected segment (with $c = 15$) using different techniques. A lower bound on the topological entropy of the Poincaré map is shown in the upper part of Figure 7 (see subsection IV C for more details). The middle part displays the first two Lyapunov exponents. As mentioned above, a positive first Lyapunov exponent suggests (after a long transient time) that the attractor is chaotic. Both indicators show the tendency to increase the complexity of the chaotic invariant set (attractor or saddle) as the value of a increases. The second Lyapunov exponent provides information in the regions where the attractor is regular – that is, it consists of an attracting periodic orbit. Therefore, if this exponent has very negative values, the periodic orbit is more stable. Conversely, if it rises to zero at one point and then falls again, this indicates a period-doubling bifurcation. A saddle-node bifurcation occurs when the first exponent drops vertically from positive values to zero and the second exponent goes from zero to negative values. Some of these bifurcations are marked with dashed green and purple segments, respectively. The bottom of the figure shows the bifurcation diagram obtained using the selected Poincaré section. This bifurcation diagram clearly shows the regular and chaotic regions identified by the Lyapunov exponents. We also use black dotted lines to mark where a new branch appears in the FRM. As can be seen, transitions from an odd number of branches to an even number of branches always occur within a regular window, where the existence of stable periodic orbits is observed. Within these windows, we have indicated the saddle-node bifurcations that give rise to the transitions. The two families of periodic orbits (stable in blue and unstable in red) that arise from these bifurcations are

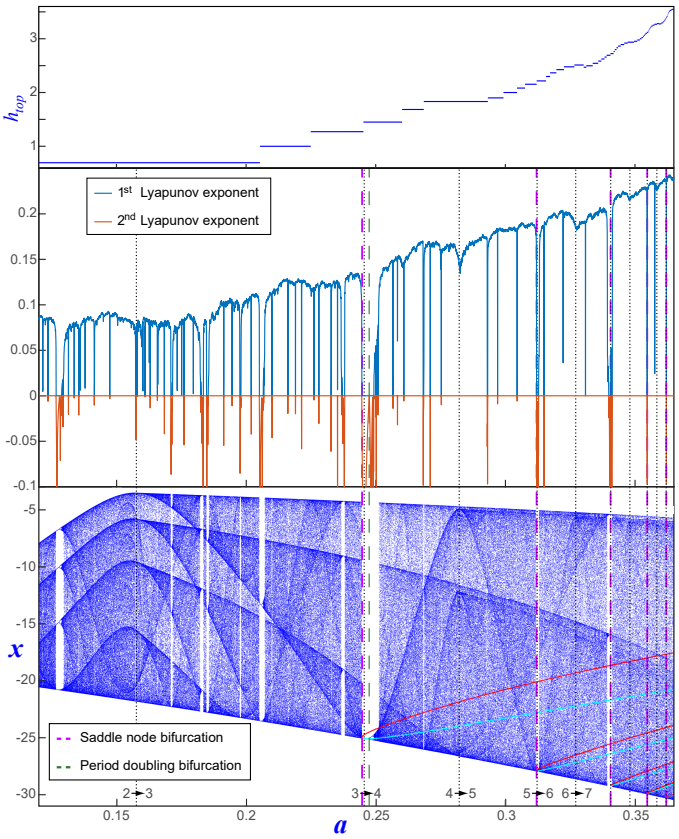

FIG. 7. Analysis of the evolution of the dynamics of the Rössler model along the selected segment in Figure 4 using different techniques. Top: lower bound on the topological entropy (see subsection IV C). Middle: Lyapunov exponents. Bottom: Bifurcation diagram representing the x-coordinate of the intersection points of the attractor with the Poincaré section Π. The dashed vertical segments indicate some saddle-node (in purple) and period-doubling (in green) bifurcations. Blue and red curves show stable and unstable families of periodic orbits born from the previous saddle-node bifurcations. The black dotted segments mark the approximate value where the FRM increases by one branch. The number of branches in the first transitions from left to right are shown above the x-axis.

also shown.

Note that although the asymptotic dynamics differ between regular and chaotic windows, there is an invariant chaotic set in both cases. This is why we can study its structure across the entire considered interval.

IV. THE MAIN RESULTS.

In this section, we fix the parameter values to $b = 0.2$ and $c = 15$. We will then study the dynamics of the Rössler system (1) for the range of parameter values $a \in \mathscr{A}$, as defined in (2).

On the Poincaré section Π defined by (4) we will use (x,z) coordinates. In this section, we present several results about the Poincaré map

$$P_a : \Pi \to \Pi \tag{5}$$

for $a \in \mathscr{A}$. The proofs of all theorems are computer-assisted and the details will be presented in Section V.

Theorem 1 *For $a \in \mathscr{A}$, the Poincaré map P_a is well defined and smooth on the set*

$$\begin{aligned}\mathscr{T} &:= [x_{\min}, x_{\max}] \times [z_{\min}, z_{\max}] \\ &= [-30.53, -3] \times [0.004, 0.011] \subset \Pi \end{aligned} \tag{6}$$

and $P_a(\mathscr{T}) \subset \operatorname{int}\mathscr{T}$.

Thus, for $a \in \mathscr{A}$, the set $\mathscr{T}$ is a trapping region for the Poincaré map P_a, containing a nonempty, compact and connected maximal invariant set

$$\mathscr{I}_a := \bigcap_{n>0} P_a^n(\mathscr{T}).$$

A. Change of topological structure of maximal invariant set.

Section III (see also Fig. 5, Fig. 6 and Fig. 7) strongly indicates that the structure of the invariant set $\mathscr{I}_a$ is changing with the parameter $a \in [a_{\min}, a_{\max}]$. In this section, we introduce some computable characteristics of the maximal invariant set and we will prove that it indeed changes when the parameter a varies.

For fixed parameter $a \in [a_{\min}, a_{\max}]$ and fixed $z \in [z_{\min}, z_{\max}]$, we define the following function:

$$f_{a,z}(x) := \pi_x P_a(x, z), \tag{7}$$

where π_x is the projection onto x-coordinate. From Theorem 1 it follows that, for all $a \in [a_{\min}, a_{\max}], z \in [z_{\min}, z_{\max}]$, the function $f_{a,z}$ is smooth on $X := [x_{\min}, x_{\max}]$ and its range is also in X.

Definition 1 *Let X be a closed interval and let $f : X \to X$ be continuous. A point $x_* \in \operatorname{int} X$ is called a* relevant extremum *of f if x_* is a strict local extremum and*

$$\min_{x \in X} f(x) \le x_* \le \max_{x \in X} f(x).$$

The cardinality of the set of relevant extrema of f is denoted by $\operatorname{relEx}(f)$.

This definition is motivated by the following observation regarding the sine model (3). Clearly, any interval $[0, N]$, where $N \ge 1$, is forward invariant for f_a. However, all local extrema located outside the range of f_a, for example satisfying $x > 1$, do not affect the structure of the invariant set in $[0,1]$. Therefore, only the extrema belonging to the range $f_a([0,N])$ are relevant to the dynamics on the invariant set, and their number provides some characteristics of the invariant set. That is, we are eliminating the transient dynamics created when the initial point is out of the interval of the invariant set. In most cases, this transient involves just one iteration of the map.

Theorem 2 *For parameter values –a– listed in (8) the number of relevant extrema of $f_{a,z} : X \to X$ defined by (7) does not depend on $z \in [z_{\min}, z_{\max}]$ and it is equal to*

a	$a_{\min}$	0.2	0.26	0.3	0.32	0.333
$\operatorname{relEx}(f_{a,z})$	1	2	3	4	5	6
a	0.345	0.35	0.356	0.36	3.62	$a_{\max}$
$\operatorname{relEx}(f_{a,z})$	7	8	9	10	11	12

(8)

The plot of $f_{a,z}$ for $z = \frac{1}{2}(z_{\min} + z_{\max})$ and $a \in \{a_{\min}, a_{\max}\}$ is shown in Fig. 8. Theorem 2 implies that, between each pair of subsequent parameter values listed in (8), a global change in the structure of $\mathscr{I}_a$ occurs.

Indeed, we have the following theorem.

Theorem 3 *Let X, Y be closed intervals, $f : X \to X$, $g : Y \to Y$ be continuous and let $\pi : X \to Y$ be a homeomorphism such that $\pi \circ f = g \circ \pi$. Then* $\operatorname{relEx}(f) = \operatorname{relEx}(g)$ *– i.e the number of relevant extrema is an invariant of conjugacy of maps defined on closed intervals.*

Proof: Consider the case of increasing π. Let $M_f = \sup_{x \in X} f(x)$ and $M_g = \sup_{y \in Y} g(y)$ and let $x_M \in X$, $y_M \in Y$ be such that $M_f = f(x_M)$ and $M_g = g(y_M)$. First, we will show that $M_g = g(\pi(x_M))$. Assume that this is not the case, that is

$$g(\pi(x_M)) < g(y_M).$$

In what follows we will skip the symbol of function composition and simply write $\pi^{-1} g \pi$ instead of $\pi^{-1} \circ g \circ \pi$. Since π is increasing, so is π^{-1}, and we have

$$\begin{aligned} M_f = f(x_M) = \big(\pi^{-1} g \pi\big) x_M = \pi^{-1}\big(\big(g\pi\big) x_M\big) < \pi^{-1}\big(g(y_M)\big) \\ = \big(\pi^{-1} g \pi\big)(\pi^{-1} y_M) = f(\pi^{-1} y_M) \end{aligned}$$

which is a contradiction. From the above, we conclude that

$$M_g = g(\pi x_M) = \pi(\pi^{-1} g \pi) x_M = (\pi f) x_M = \pi M_f.$$

Similarly, if $m_f = \inf_{x \in X} f(x)$, then $m_g = \inf_{y \in Y} g(y) = \pi m_f$.

We will now show that if x_* is a relevant extremum of f, then $y_* = \pi(x_*)$ is also a relevant extremum of g. Since $m_f \le x_* \le M_f$ and π is increasing, we have

$$m_g \le y_* \le M_g.$$

It remains to be shown that y_* is a strict extremum of g. Indeed, if U_f is an open interval containing x_* such that $f(x) < f(x_*)$ for $x \in U_f \setminus \{x_*\}$, then $U_g = \pi U_f$ is an open interval in Y containing y_*. Since π is injective, for $y \in U_g \setminus \{y_*\}$ we have $y = \pi x$ for some $x \in U_f \setminus \{x_*\}$ and

$$g(y) = \pi(\pi^{-1} g \pi) x = \pi f(x) < \pi f(x_*) = (\pi f \pi^{-1}) \pi x_* = g(y_*).$$

Similarly, we argue that, if x_* is a strict minimum for f, then so is πx_* for g.

In summary, we have shown that $\operatorname{relEx}(f) \le \operatorname{relEx}(g)$. Since the conjugacy relation is symmetric, we can repeat the arguments for π^{-1} and conclude that $\operatorname{relEx}(g) \le \operatorname{relEx}(f)$.

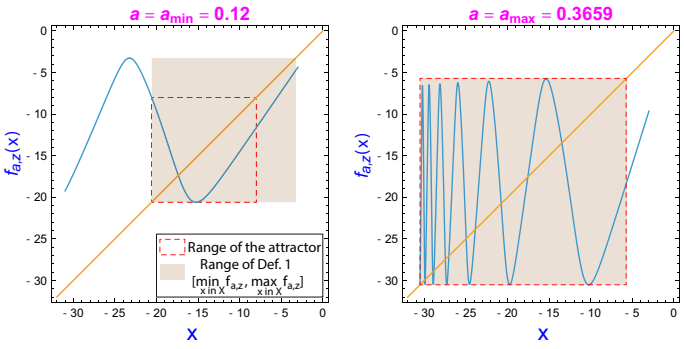

FIG. 8. Plot of the function $f_{a,z} : [x_{\min}, x_{\max}] \to [x_{\min}, x_{\max}]$ for $z = z_{\text{mid}} := \frac{1}{2}(z_{\min} + z_{\max})$ and $a = a_{\min}$ (left) and $a = a_{\max}$ (right). It is a numerical evidence that $\text{relEx}(f_{a_{\min}, z_{\text{mid}}}) = 1$ and $\text{relEx}(f_{a_{\max}, z_{\text{mid}}}) = 12$. The range of Def. 1($[\min_{x\in X} f_{a,z}, \max_{x\in X} f_{a,z}]$) is shown in a brown rectangle. To compare with the range of the attractor (see the bottom plots of Fig. 5), we plot them as a red rectangle.

To prove the case of decreasing π, let us define

$$\widetilde{Y} = \{-y : y \in Y\},$$
$$\widetilde{\pi}(x) = -\pi(x) \quad \text{and}$$
$$\widetilde{g} \ : \ \widetilde{Y} \ni y \to -g(-y) \to \widetilde{Y}.$$

Clearly, $\widetilde{\pi}$ is an increasing homeomorphism between X and $\widetilde{Y}$ which conjugates f and $\widetilde{g}$. Therefore, $\text{relEx}(f) = \text{relEx}(\widetilde{g}) = \text{relEx}(g)$.

□

B. Saddle-node bifurcations.

In the sine model (3), we observed that some of the relevant extrema (in particular, the maxima) are created via saddle-node bifurcations. Such a bifurcation creates a stable periodic orbit which coexists with a chaotic invariant set. As can be seen in Fig. 7, this is also observed in the Rössler model (1). In this section, we will focus on this scenario.

Consider the following function.

$$g(x,z,a) = (P_a(x,z) - (x,z), \det(DP_a(x,z) - \text{Id})). \quad (9)$$

Clearly, $g(x,z,a) = 0$ if (x,z) is a fixed point of P_a and $\lambda = 1$ is an eigenvalue of $DP_a(x,z)$. Using the standard Newton method applied to g, we have found approximate zeros of g in the parameter range $[a_{\min}, a_{\max}]$ – see Table I.

i	x_i	z_i	a_i
1	-24.98615641824929	0.0050036959553767296	0.2445890212249042
2	-27.90101006311546	0.004663547021688063	0.3119866509093180
3	-29.22211573599117	0.004524155280447693	0.3405236989996505
4	-29.89377365336397	0.004456435009829962	0.3546641965836549
5	-30.25817997684925	0.004420535075303823	0.3623180183723328

TABLE I. Approximate bifurcation points (x_i, z_i, a_i) of the Poincaré map P_a.

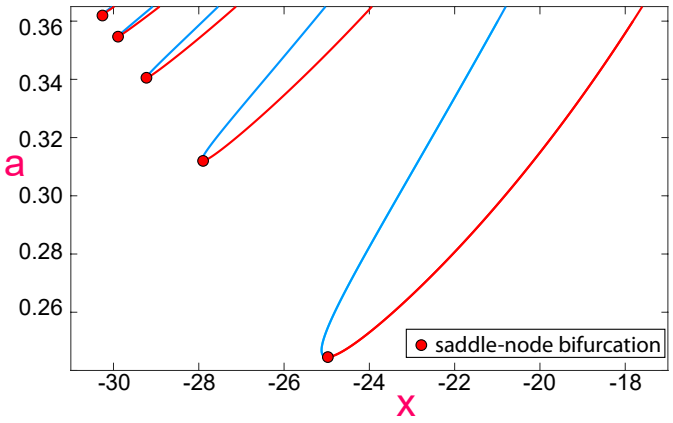

FIG. 9. Saddle-node bifurcations and branches of fixed points of P_a resulting from Theorem 4.

Theorem 4 *The Poincaré map P_a undergoes a saddle-node bifurcation at the points (x_i^*, z_i^*, a_i^*), $i = 1, \ldots, 5$ with*

$$|x_i^* - x_i| \le 3 \cdot 10^{-11}, \quad |z_i^* - z_i| \le 10^{-14}, \quad |a_i^* - a_i| \le 6 \cdot 10^{-14}, \quad (10)$$

where (x_i, z_i, a_i) are listed in Table I. Moreover,

$$\text{Sp}\left(DP_{a_i^*}(x_i^*, z_i^*)\right) = \{1, \lambda_i\} \quad \text{and} \quad |\lambda_i| < 2 \cdot 10^{-4}.$$

For $i = 1, \ldots, 5$ there are two different and continuous branches of fixed points of P_a, denoted by $L_i(a)$ and $R_i(a)$ and parameterised by $a \in [a_i^*, a_{\max}]$, such that $L_i(a_i^*) = R_i(a_i^*) = (x_i^*, z_i^*)$ and $L_i(a) \neq R_i(a)$ for $a > a_i^*$.

Figure 9 shows the bifurcation diagram of the fixed points of P_a, as derived from Theorem 4. The turning points correspond to the saddle-node bifurcation, giving rise to a stable and an unstable branch of fixed points of P_a. Since the absolute value of the non-bifurcation eigenvalue of $DP_{a_i^*}(x_i^*, z_i^*)$ at each bifurcation point is less than 1, an attracting periodic orbit is created for parameter values slightly above a_i^*, $i = 1, \ldots, 5$, – see Fig. 7. In the next section we will prove that it coexists with an invariant set on which the topological entropy of P_a is positive.

C. Symbolic dynamics and topological entropy.

In the scenario presented for the sine model (3), we have seen that an increasing number of relevant extrema leads to an increase in the topological entropy of the system. Here, we address the same question for the Poincaré map P_a.

The following definitions are standard (see for example Guckenheimer and Holmes [53] and Katok and Hasselblatt [9]). Let us fix $k > 0$ and let $\{M_{ij}\}_{i,j=1,\ldots,k}$ be $k \times k$ matrix, such that $M_{ij} \in \{0, 1\}$. We define Σ_M by

$$\Sigma_M = \{c \in \{1, 2, \ldots, k\}^{\mathbb{Z}} \mid M_{c_i c_{i+1}} = 1 \ \forall i \in \mathbb{Z}\}. \quad (11)$$

We define a shift map σ on Σ_M by

$$\sigma(c)_i = c_{i+1}, \quad \forall i \in \mathbb{Z}.$$

The pair (Σ_M, σ) is called a *subshift of finite type with transition matrix M* or a *topological Markov chain*.

The shift dynamics can easily be visualised as a finite directed graph. The constant k is often called *the number of symbols*, but it can also be seen as the number of vertices in a directed graph. The transition matrix M defines the edges of this graph ($M_{ij} = 1$ iff there is an edge from vertex i to vertex j). A biinfinite sequence, $(c_i)_{i\in\mathbb{Z}} \in \Sigma_M$, defines a biinfinite path in this graph. Clearly, the complexity of the shift dynamics (i.e. the number of different trajectories or different possible paths on the graph) cannot decrease when new edges (i.e. new nonzero coefficients in M) are added to the graph.

The following theorem is a classical result about the entropy of topological Markov chains.

Theorem 5 (Katok and Hasselblatt[9] (Prop. 3.2.5)) *The topological entropy of the shift map* (Σ_M, σ) *is equal to*

$$h_{top}(\sigma) = h_{top}(M) = \max_{\lambda \in \mathrm{Sp}(M)} \log(|\lambda|).$$

It is well known that the topological entropy is an invariant of conjugacy of maps. In the case of semiconjugacy, however, we obtain only a one-sided inequality. Therefore, showing semiconjugacy of a map f to the shift dynamics σ is a way to obtain a lower bound on the topological entropy $h_{top}(f) \geq h_{top}(\sigma)$.

Theorem 6 *For all parameter values* $a \in [a_{\min}, a_{\max}]$*, there is an invariant subset* $\mathscr{H}_a \subset \mathscr{T}$ *for* P_a*, such that* $P_a|_{\mathscr{H}_a}$ *is semiconjugated to a subshift of finite type. The associated directed graphs of possible transitions are connected and the number of their vertices varies from* 2 *for* $a = a_{\min}$ *to* 13 *for* $a = a_{\max}$*. A lower bound on the topological entropy of* P_a *in different parameter ranges is listed in Table II.*

Remark 7 *The data returned by the validation algorithm (described in Section V) and presented in Table II is a lower bound on the complexity of the dynamics of* P_a *restricted to some invariant set* $\mathscr{H}_a$ *(not necessarily the maximal invariant set). Based on the approximate minima of the first iterate of* $f_{a,z}$ *given by (7), the algorithm constructs and validates semiconjugacy of* P_a *to a subshift of finite type. To apply computer-assisted reasoning, we need a margin for accumulated errors arising from overestimation in the validated integration of ODEs and, most importantly, the fact that the algorithm always works over a range of parameters rather than a single parameter value. Therefore, changes in topological entropy observed in non-validated numerical simulations always appear for slightly smaller values of the parameter than those presented in Table II. Considering higher order iterates of* P_a *would, perhaps, return a more accurate lower bound on topological entropy, but would require very large CPU time.*

List of all transition matrices M_i, $i = 1, \ldots, 86$ is available in the supplementary material for this article[54]. For $a = a_{\min}$, the transition matrix is equal to

$$M_1 = \begin{bmatrix} 0 & 1 \\ 1 & 1 \end{bmatrix}$$

with $h_{top}(M_1) = \log_2 \frac{1+\sqrt{5}}{2} \approx 0.6942419136306173$. When a grows, the number of symbols increases and the leading transition matrices in the sequence are

$$M_2 = \begin{bmatrix} 0 & 1 & 1 \\ 1 & 1 & 1 \\ 1 & 0 & 0 \end{bmatrix}, \quad M_3 = \begin{bmatrix} 0 & 1 & 1 \\ 1 & 1 & 1 \\ 1 & 1 & 0 \end{bmatrix},$$

$$M_4 = \begin{bmatrix} 0 & 1 & 1 \\ 1 & 1 & 1 \\ 1 & 1 & 1 \end{bmatrix}, \quad M_5 = \begin{bmatrix} 0 & 1 & 1 & 1 \\ 1 & 1 & 1 & 1 \\ 1 & 1 & 1 & 1 \\ 0 & 0 & 0 & 1 \end{bmatrix}, \ldots$$

For $a \in [a_{86}, a_{\max}]$ the algorithm returned semiconjugacy of $P_a|_{\mathscr{H}_a}$ to a subshift of finite type with the transition matrix equal to

$$M_{86} = \begin{bmatrix} 0&0&0&0&1&1&1&1&1&1&1&1&1 \\ 1&1&1&1&1&1&1&1&1&1&1&1&1 \\ 1&1&1&1&1&1&1&1&1&1&1&1&1 \\ 1&1&1&1&1&1&1&1&1&1&1&1&1 \\ 1&1&1&1&1&1&1&1&1&1&1&1&1 \\ 1&1&1&1&1&1&1&1&1&1&1&1&1 \\ 1&1&1&1&1&1&1&1&1&1&1&1&1 \\ 1&1&1&1&1&1&1&1&1&1&1&1&1 \\ 1&1&1&1&1&1&1&1&1&1&1&1&1 \\ 1&1&1&1&1&1&1&1&1&1&1&1&1 \\ 1&1&1&1&1&1&1&1&1&1&1&1&1 \\ 1&1&1&1&1&1&1&1&1&1&1&1&1 \\ 1&1&1&1&0&0&0&0&0&0&0&0&0 \end{bmatrix} \qquad (12)$$

and with $h_{top}(M_{86}) = \log_2 12 \approx 3.5849625007211562$.

V. COMPUTER-ASSISTED PROOFS OF MAIN RESULTS.

The proofs of Theorems 1, 2, 4 and 6 are computer assisted – that is, we used a computer to obtain guaranteed bounds on Poincaré map P_a and its derivatives with respect to the arguments and parameter. These bounds are then used in the proofs of Theorems 1, 2, 4 and 6.

We used the CAPD library[25], which is a general purpose C++ tool for rigorous numerical analysis of dynamical systems. The library implements algorithms for the integration of (higher order) variational equations for ODEs[26–28] as well as the computation of bounds on Poincaré maps and their derivatives[29].

We would like to emphasise that the computations related to Theorems 1, 2, 4 and 6 are quite demanding – total time of computation was approximately 5 hours on a computer running 144 parallel threads. However, most of this time was spent obtaining bounds for the parameter range $a \geq 0.34$. Below this value, the program can easily be run on a laptop computer with 16 cores.

i	a_i	k_i	$h_{top}(\sigma_i)$	i	a_i	k_i	$h_{top}(\sigma_i)$	i	a_i	k_i	$h_{top}(\sigma_i)$	i	a_i	k_i	$h_{top}(\sigma_i)$	i	a_i	k_i	$h_{top}(\sigma_i)$
1	0.12	2	0.69424	19	0.326625	6	2.51135	37	0.350887	9	2.97691	55	0.357549	10	3.26958	73	0.362596	12	3.44169
2	0.205347	3	1	20	0.330221	6	2.47024	38	0.351899	9	3	56	0.358474	10	3.28097	74	0.362686	12	3.45506
3	0.224948	3	1.27155	21	0.331218	7	2.49716	39	0.352489	9	3.02203	57	0.35939	10	3.26655	75	0.36276	12	3.46804
4	0.245266	3	1.44998	22	0.3337	7	2.5431	40	0.353056	9	3.0431	58	0.359478	11	3.27655	76	0.362864	12	3.48066
5	0.248131	4	1.44998	23	0.335811	7	2.58496	41	0.353415	9	3.06331	59	0.360131	11	3.29216	77	0.36296	12	3.49295
6	0.26019	4	1.68451	24	0.337042	7	2.62346	42	0.353793	9	3.08272	60	0.360669	11	3.30727	78	0.363111	12	3.50491
7	0.268539	4	1.8325	25	0.338258	7	2.65915	43	0.354069	9	3.10141	61	0.360981	11	3.32192	79	0.36327	12	3.51658
8	0.282119	4	1.8325	26	0.339076	7	2.69244	44	0.354117	9	3.08272	62	0.361279	11	3.33614	80	0.363562	12	3.52796
9	0.293257	5	1.89996	27	0.340544	7	2.72367	45	0.354156	9	3.10141	63	0.361464	11	3.34995	81	0.363962	12	3.53908
10	0.299273	5	2	28	0.340679	8	2.72367	46	0.354669	9	3.11942	64	0.361652	11	3.36338	82	0.364342	12	3.54654
11	0.304501	5	2.08272	29	0.341748	8	2.76289	47	0.354711	10	3.11942	65	0.361687	11	3.34995	83	0.365012	13	3.55392
12	0.307588	5	2.15363	30	0.342225	8	2.79881	48	0.355138	10	3.14117	66	0.361737	11	3.36338	84	0.365385	13	3.56449
13	0.312085	5	2.21591	31	0.34285	8	2.83202	49	0.355319	10	3.16189	67	0.361862	11	3.37645	85	0.365689	13	3.57483
14	0.312612	6	2.21591	32	0.34345	8	2.86293	50	0.355538	10	3.1817	68	0.362	11	3.38918	86	0.365865	13	3.58496
15	0.315698	6	2.29786	33	0.344494	8	2.89187	51	0.355729	10	3.20067	69	0.362107	11	3.40159				
16	0.317262	6	2.36634	34	0.345848	8	2.9191	52	0.356014	10	3.21888	70	0.362319	11	3.4137				
17	0.31969	6	2.42553	35	0.347179	8	2.93608	53	0.356308	10	3.2364	71	0.362335	12	3.4137				
18	0.322604	6	2.47787	36	0.349673	9	2.95264	54	0.356837	10	3.25328	72	0.36252	12	3.42792				

TABLE II. A lower bound on the topological entropy of P_a in different subintervals of the parameter range $[a_{\min}, a_{\max}]$. For the parameter values $a \in [a_i, a_{i+1}]$ with $a_{87} = a_{\max}$, $P_a|_{\mathscr{H}_a}$ is semiconjugated to a shift dynamics σ_i on k_i symbols with topological entropy $h_{top}(\sigma_i)$. See also Fig. 7 (top panel).

A. Proof of Theorem 1.

Recall that the parameter range $\mathscr{A}$ is defined in (2) and the trapping region $\mathscr{T}$ is defined in (6). We must show that, for $a \in [a_{\min}, a_{\max}]$, the Poincaré map (5) is defined on $\mathscr{T}$ and that $P_a(\mathscr{T}) \subset \operatorname{int}\mathscr{T}$.

The validation of the inclusion $P_a(\mathscr{T}) \subset \operatorname{int}\mathscr{T}$ is split into two steps.

Step 1. First, we validate that the Poincaré map $P_a(u)$ is defined for all $a \in \mathscr{A}$ and for all $u \in \mathscr{T}$. Therefore, no restrictions are given on obtained bounds on $P_a(u)$. For this purpose, we cover the set $\mathscr{A} \times \mathscr{T}$ by some initial grid of boxes $A_i \times X_i \times Z_i$, $i = 1, \ldots, N$. Then, for each i, we call a general routine from the CAPD library[25] that computes a bound for $P_{A_i}(X_i, Z_i)$. According to the construction of the algorithm from the CAPD library, if the procedure returns (any) bound, then the Poincaré map exists and, by implicit function theorem, it is smooth on its domain. Otherwise, the algorithm throws an exception. In this case, we bisect the set $A_i \times X_i \times Z_i$ in the (a,x) coordinates and repeat the computation.

This subdivision process is repeated until the existence of the Poincaré map is validated for each set in the subdivision, or until the maximal depth of subdivision is exceeded. In the latter case, we return `Failure` and stop the computation.

Running this algorithm, we found a (non-uniform) cover of $\mathscr{A} \times \mathscr{T}$, consisting of 36316641 boxes, on which the existence of the Poincaré map has been validated.

Step 2. In the second step, we check that $P_a(\partial\mathscr{T}) \subset \operatorname{int}\mathscr{T}$ for $a \in \mathscr{A}$. After adaptive subdivision, as in the first step, we found a (non-uniform) cover $A_i \times X_i \times Z_i$, $i = 1, \ldots, 9299383$ of $\mathscr{A} \times \partial\mathscr{T}$, such that $P_{A_i}(X_i \times Z_i) \subset \operatorname{int}\mathscr{T}$ for $i = 1, \ldots, 9299383$.

Since P_a is a diffeomorphism onto its image, by the Jordan Theorem, we conclude that $P_a(\mathscr{T}) \subset \operatorname{int}\mathscr{T}$, for $a \in \mathscr{A}$. □

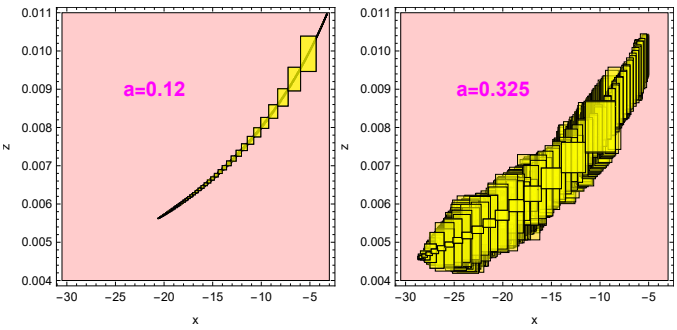

FIG. 10. Trapping region $\mathscr{T}$ is shown in pink. Computed bound on $P_a(\partial\mathscr{T})$ for $a = a_{\min}$ (left) and $a = 0.325$ (right) is shown in yellow.

Figure 10 shows the obtained bound on $P_a(\partial\mathscr{T})$ for $a = a_{\min}$ and $a = 0.325$.

B. Proof of Theorem 2.

Let $X = [x_{\min}, x_{\max}]$ and $Z = [z_{\min}, z_{\max}]$. In Theorem 2 we need to count the number of relevant extrema of the map $f_{a,z} : X \to X$, which is defined in (7). For each parameter value listed in (8), we run an algorithm consisting of the following steps.

- Using a standard bisection search, we localise approximate extrema of $f_{a,z}$ in X for

$$z \in \{z_{\min}, z_{\max}, \frac{1}{2}(z_{\min} + z_{\max})\}.$$

Denote this (finite) set by E.

- We initially cover X by subintervals X_i.
- If $X_i \cap E = \emptyset$, we compute bounds for $f_{a,Z}(X_i)$ and $f'_{a,Z}(X_i)$. If the computed bound for $f'_{a,Z}(X_i)$ contains zero, the interval X_i is bisected and the procedure repeats until the bound for the derivative does not contain zero or the subdivision depth is exceeded.
- Similarly, if $X_i \cap E \neq \emptyset$ we request computation of bounds on $f_{a,Z}(X_i)$, $f'_{a,Z}(X_i)$ and $f''_{a,Z}(X_i)$. If the computed bound for $f''_{a,Z}(X_i)$ contains zero, the interval X_i is bisected and the process is repeated until the bound for the second derivative does not contain zero, or the subdivision depth is exceeded.

By the construction of the algorithm, if it stops and all tasks return nonzero bounds for first or second derivative of $f_{a,Z}$, respectively, then the domain X is covered by intervals Y_i on which either $f_{a,Z}$ is monotone or convex/concave.

Table III provides a sample output of the algorithm for $a = a_{\max}$. The bounds for $f'_{a,z}$ and $f''_{a,z}$ show that the function has exactly 12 local extrema in X. From the bound for $f_{a,z}$ (second column) and Theorem 1, we can conclude that

$$-30.53 \leq \inf_{x\in X} f_{a,Z}(x) \leq -30.52 \quad \text{and}$$
$$-5.75 \leq \sup_{x\in X} f_{a,Z}(x) \leq -5.73.$$

These bounds imply that all found extrema are relevant, and thus $\mathrm{relEx}(f_{a_{\max},z}) = 12$ for $z \in [z_{\min}, z_{\max}]$.

The output of the program for the remaining parameter values (8) is given in the supplementary material[54]. From the obtained bounds, we can determine the number of relevant extrema of $f_{a,z}$ as given in (8). □

Remark 8 *Note that computing $f''_{a,z}$ requires the costly integration of the second order variational equation for (1).*

C. Proof of Theorem 4.

Before we describe the algorithm for validating the bifurcation and continuation of fixed points of P_a, we recall some standard tools for validating the existence of branches of zeros of smooth functions.

For a smooth function $F : D \subset \mathbb{R}^m \times \mathbb{R}^n \to \mathbb{R}^n$ and an interval vector (Cartesian product of closed intervals) $A \times X \subset D$, we set

$$[D_X F(A,X)] := \mathrm{convexHull}\{D_x F(a,x) : a \in A, x \in X\}.$$

Theorem 9 (Interval Newton Method[17]) *Let $F : D \subset \mathbb{R}^n \to \mathbb{R}^n$ be a smooth function, $X \subset D$ an interval vector and $x_0 \in \mathrm{int}X$. If $[D_X F(X)]$ is nonsingular and*

$$N(F,X,x_0) := x_0 - [D_X F(X)]^{-1} \cdot F(x_0) \subset \mathrm{int}X, \qquad (13)$$

then F has a unique zero x^* in the set X. Moreover, $x^* \in N(F,X,x_0)$.

The following is a straightforward extension of the Interval Newton Method (INO) to the case of parameter dependent functions.

Theorem 10 (Parameterized INO[55]) *Let $F : D \subset \mathbb{R}^m \times \mathbb{R}^n \to \mathbb{R}^n$ be a smooth function, $A \times X \subset D$ be an interval vector and $x_0 \in \mathrm{int}X$. If $[D_X F(A,X)]$ is nonsingular and*

$$N = N(F,A,X,x_0) := x_0 - [D_X F(A,X)]^{-1} \cdot F(A,x_0) \subset \mathrm{int}X, \qquad (14)$$

then there is a smooth function $g : A \to N \subset X$ such that $F(g(x),x) \equiv 0$. Moreover, if $F(a,x) = 0$ for some $(a,x) \in A \times X$, then $a = g(x)$.

Let us fix the parameter $a = a_i$ as shown in Table I. Below, in the description of the algorithm, we provide some data (numbers) obtained in the validation of the first bifurcation point (x_1, z_1, a_1) – the remaining can be found in the supplementary material[54].

The algorithm, which validates the existence of a saddle-node bifurcation and two branches of fixed points as in Theorem 4, consists of the following steps.

Step 1: Validation of the bifurcation point. Define

$$u_i = (x_i, z_i, a_i),$$
$$W_i = u_i + [-1,1] \cdot (3 \cdot 10^{-11}, 10^{-14}, 6 \cdot 10^{-14}).$$

Let g be defined as in (9). Using algorithms from the CAPD library, we compute the Interval Newton Operator (13) and check that $N(g, W_i, u_i) \subset \mathrm{int}W_i$. Thus, by means of Theorem 9, there exists a unique $(x_i^*, z_i^*, a_i^*) \in W_i$ such that

$$P_{a_i^*}(x_i^*, z_i^*) = (x_i^*, z_i^*) \quad \text{and} \quad 1 \in \mathrm{Sp}(DP_{a_i^*}(x_i^*, z_i^*)).$$

Applying Gershgorin estimate to the obtained bound on the derivative $DP_{a_i^*}(x_i^*, z_i^*)$ we have checked that the second eigenvalue λ_i of $DP_{a_i^*}(x_i^*, z_i^*)$ satisfies $|\lambda_i| \leq 2 \cdot 10^{-4}$.

Step 2: Validation of a short curve of fixed points of P_a near (x_i^*, z_i^*, a_i^*).

Define the map $F(x,z,a) = P_a(x,z) - (x,z)$. We impose that the set of zeros of this function can be locally parameterised near (x_i^*, z_i^*, a_i^*) as a smooth curve of the form

$$u(x) = (x, z(x), a(x)).$$

To apply the Interval Newton Method (Theorem 10), we define an explicit set

$$D_i = X_i \times Z_i \times A_i = (x_i, z_i, a_i) + [-1,1] \cdot (\Delta_i^x, \Delta_i^z, \Delta_i^a).$$

Using algorithms from the CAPD library, we compute the Interval Newton Operator (14) for the map F and check that

$$N(F, X_i, D_i, (x_i, z_i, a_i)) \subset \mathrm{int}\,(Z_i \times A_i).$$

From Theorem 9, we conclude that all zeros of F in D_i form the graph of a smooth function $u(x) = (x, z(x), a(x))$, $x \in x_i + [-1,1]\Delta_i^x$.

The actual (hand adjusted) diameters for $i = 1$ are

$$(\Delta_1^x, \Delta_1^z, \Delta_1^a) = (5 \cdot 10^{-4}, 3 \cdot 10^{-7}, 2 \cdot 10^{-5}).$$

x	$f_{a,z}(x)$	$f'_{a,z}(x)$	$f''_{a,z}(x)$
$[-30.530000000000000, -30.234918150004624]$	$[-30.19, -6.57]$	$[0.001, 184]$	–
$[-30.234918150004624, -30.234487860323142]$	$[-6.58, -6.57]$	$[-0.72, 0.58]$	$[-1326, -325]$
$[-30.234487860323142, -29.926850797851111]$	$[-30.44, -6.57]$	$[-230, -0.001]$	–
$[-29.926850797851111, -29.925276370697883]$	$[-30.44, -30.43]$	$[-0.89, 2.63]$	$[101, 1193]$
$[-29.925276370697883, -29.433781614317695]$	$[-30.44, -6.47]$	$[0.0007, 122]$	–
$[-29.433781614317695, -29.432550550415712]$	$[-6.48, -6.47]$	$[-0.77, 0.59]$	$[-578, -68]$
$[-29.432550550415712, -28.936271584068677]$	$[-30.45, -6.47]$	$[-138, -0.009]$	–
$[-28.936271584068677, -28.933364707472052]$	$[-30.45, -30.44]$	$[-0.87, 1.87]$	$[73, 418]$
$[-28.933364707472052, -28.134274742819773]$	$[-30.45, -6.36]$	$[0.006, 75.5]$	–
$[-28.134274742819773, -28.129878233661032]$	$[-6.37, -6.36]$	$[-1.2, 0.66]$	$[-227, -18]$
$[-28.129878233661032, -27.315443495151083]$	$[-30.47, -6.36]$	$[-86.7, -0.04]$	–
$[-27.315443495151083, -27.309055771711787]$	$[-30.47, -30.45]$	$[-1.66, 1.72]$	$[23, 156]$
$[-27.309055771711787, -25.978724324556815]$	$[-30.49, -6.23]$	$[0.004, 31.4]$	–
$[-25.978724324556815, -25.969275484986035]$	$[-6.24, -6.23]$	$[-0.83, 0.73]$	$[-79, -9.6]$
$[-25.969275484986035, -24.583975022884346]$	$[-30.49, -6.23]$	$[-49.91, -0.01]$	–
$[-24.583975022884346, -24.573109921220805]$	$[-30.5, -30.45]$	$[-1.1, 1.2]$	$[7.2, 56]$
$[-24.573109921220805, -22.263096727912796]$	$[-30.48, -6.05]$	$[0.01, 17.7]$	–
$[-22.263096727912796, -22.244978977377045]$	$[-6.06, -6.05]$	$[-0.68, 0.71]$	$[-29.2, -0.2]$
$[-22.244978977377045, -19.75178920778561]$	$[-30.5, -6.05]$	$[-21.8, -0.02]$	–
$[-19.75178920778561, -19.732234778220185]$	$[-30.5, -30.49]$	$[-0.36, 0.36]$	$[0.15, 19]$
$[-19.732234778220185, -15.379434543948365]$	$[-30.5, -5.74]$	$[0.0007, 8.1]$	–
$[-15.379434543948365, -15.345294934267804]$	$[-5.75, -5.73]$	$[-0.51, 0.51]$	$[-7.9, -0.2]$
$[-15.345294934267804, -10.256384670433105]$	$[-30.53, -5.74]$	$[-7.8, -0.004]$	–
$[-10.256384670433105, -10.216471648755972]$	$[-30.54, -30.52]$	$[-0.2, 0.2]$	$[1.6, 2.6]$
$[-10.216471648755972, -3]$	$[-30.54, -9.63]$	$[0.01, 3.3]$	–

TABLE III. Bounds for $f_{a,z}$ and its derivatives for $a = a_{\max}$ and $z \in [z_{\min}, z_{\max}]$.

The computed bound on the Interval Newton Operator (14) is

$$N(F, X_1, D_1, (x_1, z_1, a_1)) \subset (z_1, a_1) - [-1, 1](2.1 \cdot 10^{-7}, 1.15 \cdot 10^{-5}).$$

Step 3: Validation of the saddle-node bifurcation point (x_i^*, z_i^*, a_i^*).

From **Step 1** and **Step 2** and the uniqueness property of the Interval Newton Method, we know that $a_i^* = a(x_i^*)$ and $z_i^* = z(x_i^*)$. We would like to show that the function $a(x)$ has a unique minimum in x_i^* and is a convex function in X_i. For this purpose, we again apply Theorem 9 to obtain tighter bounds on $a'(x_i - \Delta_i^x)$ and $a'(x_i + \Delta_i^x)$. We then check if these derivatives have opposite signs. For $i = 1$, we obtain bounds

$$a'(x_1 - \Delta_1^x) \in [-3.3, -3.2] \cdot 10^{-7},$$
$$a'(x_1 + \Delta_1^x) \in [3.2, 3.3] \cdot 10^{-7}.$$

Finally, we check that $a''(X_i) > 0$ and thus a is a convex function. For $i = 1$, we obtain a bound

$$a''(X_1) \subset [0.05, 0.08].$$

The derivatives a' and a'' are computed by differentiating the identity

$$F(x, z(x), a(x)) \equiv 0. \tag{15}$$

From all these bounds, we conclude that the function $a(x)$ has a unique minimum in X_i, say $\widehat{a}_i = a(\widehat{x}_i)$ with the corresponding $\widehat{z}_i = z(\widehat{x}_i)$. Our aim is to show that $\widehat{x}_i = x_i^*$. Differentiating (15) and setting $\det\left(DP_{a_i^*}(x_i^*, z_i^*) - \mathrm{Id}\right) = 0$ gives $a'(x_i^*) = 0$. Since $a''(X_i) > 0$, the derivative a' is monotone in X_i, so $0 = a'(\widehat{x}_i) = a'(x_i^*)$ implies that $x_i^* = \widehat{x}_i$.

From the above considerations, we conclude that the set of fixed points of P_a in D_i can be parameterised as the union of the graphs of two functions

$$L : [a_i^*, a_i(x_i - \Delta_i^x)] \ni a \to (x(a), z(a)) \in X \times Z,$$
$$R : [a_i^*, a_i(x_i + \Delta_i^x)] \ni a \to (x(a), z(a)) \in X \times Z.$$

Step 4: Continuation of the branches L and R until $a = a_{\max}$.

In this step, we perform an adaptive subdivision of the parameter ranges

$$A_i^L = [a_i(x_i - \Delta_i^x), a_{\max}] \quad \text{and}$$
$$A_i^R = [a_i(x_i + \Delta_i^x), a_{\max}].$$

We start from an initial cover of A_i^L and A_i^R by intervals and try to validate the existence of a branch of zeros of F in each subinterval using Interval Newton Operator – see Theorem 10. If the verification step fails, we bisect the parameter range and repeat the computation. This subdivision process stops either when we can validate the existence of a branch of fixed points for P_a in each subinterval, or when the maximal depth of subdivisions is exceeded.

In each case $i = 1,\dots,5$, the algorithm returned covers

$$A_i^L = [a_i(x_i - \Delta_i^x), a_{\max}] \subset \bigcup_{k=1}^{K_i^L} [a_{i,k-1}^L, a_{i,k}^L] \quad \text{and}$$

$$A_i^R = [a_i(x_i + \Delta_i^x), a_{\max}] \subset \bigcup_{k=1}^{K_i^R} [a_{i,k-1}^R, a_{i,k}^R]$$

such that, on each subinterval, the existence of a branch of fixed points of P_a has been validated. In each case $i = 1,\dots,5$, the number of subintervals, K_i^L and K_i^R, exceeds 10^4.

Step 5: Verification of smoothness of branches L and R.

We must check whether the segments of L and R on each subinterval merge into a smooth curve. For this purpose, we additionally compute (using again the Interval Newton Method and Theorem 9) a tight bound on $L(a_{i,k}^L)$, $k = 1,\dots,K_L - 1$. We then show that $L(a_L^k)$ belongs to the computed bounds for the segments $[a_{i,k-1}^L, a_{i,k}^L]$ and $[a_{i,k}^L, a_{i,k+1}^L]$. From the uniqueness property of the Interval Newton Method, we conclude that these segments merge into a continuous curve which is smooth by the implicit function theorem. Similarly for the branch R.

Finally, we have to repeat the argument to obtain smoothness at $a_{i,0}^L = a_i(x_i - \Delta_i^x)$ and $a_{i,0}^R = a_i(x_i + \Delta_i^x)$. This time, we must use a bound from the verification on the curve of fixed points $u(x)$ from **Step 2** and parameterized by $x \in X_i$.

□

D. Proof of Theorem 6.

The proof of Theorem 6 relies on the automatic (algorithmic) construction and verification of semiconjugacy of P_a to a subshift of finite type. For this purpose, we use the method of covering relations introduced for two-dimensional maps by Zgliczyński [16] and later extended to multidimensional case by Zgliczyński and Gidea [56]. This method is also closely related to the correctly aligned windows method by Easton [57].

Since P_a is a two-dimensional map, we recall the definition from Zgliczyński [16] here and simplify it for the settings of the Poincaré map P_a.

Definition 2 *Let $|N| = [a,b] \times [c,d]$ be a rectangle and put*

$$\begin{aligned} N^{le} &= \{a\} \times [c,d], \\ N^{re} &= \{b\} \times [c,d], \\ N^{l} &= (\infty, a) \times [c,d], \\ N^{r} &= (b, \infty) \times [c,d], \\ N^{s} &= \mathbb{R} \times (c,d). \end{aligned}$$

The tuple $N = (|N|, N^{le}, N^{re}, N^l, N^r, N^s)$ is called an h-set.

Assume that $N_1,\dots,N_k$, $k \geq 1$ are pairwise disjoint h-sets. Put $D = \bigcup_{i=1}^k |N_i|$ and let $f : D \to \mathbb{R}^2$ be continuous. Denote by $\mathrm{Inv}(f,D) \subset D$ the maximal invariant set for f in D. Since the sets are pairwise disjoint, for any $x \in \mathrm{Inv}(f,D)$ there is a unique sequence $(x_{i_j})_{j\in\mathbb{Z}}$ such that

- $x_{i_0} = x$,
- $x_{i_j} \in |N_{i_j}|$, $j \in \mathbb{Z}$,
- $f(x_{i_j}) = x_{i_{j+1}}$, $j \in \mathbb{Z}$.

The above defines a mapping $\pi : \mathrm{Inv}(f,D) \ni x \to (i_j)_{j\in\mathbb{Z}} \in \{1,\dots,k\}^{\mathbb{Z}}$.

Definition 3 *Let $f : D \subset \mathbb{R}^2 \to \mathbb{R}^2$ be a continuous map and let N_1, N_2 be h-sets (can be the same). We say that the set N_1 f-covers N_2, denoted by $N_1 \overset{f}{\Longrightarrow} N_2$, if $f(|N_1|) \subset N_2^s$ and*

1. *either $f(N_1^{re}) \subset N_2^r$ and $f(N_1^{le}) \subset N_2^l$*
2. *or $f(N_1^{re}) \subset N_2^l$ and $f(N_1^{le}) \subset N_2^r$.*

The following theorem is a special case of results from Refs.[16,56,57] about the method of covering relations.

Theorem 11 *Let $N_1,\dots,N_k$ be pairwise disjoint h-sets and let $M \subset \mathbb{R}^{k\times k}$ be a transition matrix defined in the following way*

$$M_{ij} = \begin{cases} 1 & \text{if } N_i \overset{f}{\Longrightarrow} N_j, \\ 0 & \text{otherwise}. \end{cases}$$

Put $\mathscr{I} = \mathrm{Inv}(f, \bigcup_{i=1}^k |N_i|)$. Then $\Sigma_M \subset \pi(\mathscr{I})$ (see (11) for the definition of Σ_M). Moreover, if $c = (i_j) \in \Sigma_M$ is a periodic sequence of principal period n, then there exists $x \in \pi^{-1}(c) \in \mathscr{I}$, such that $f^n(x) = x$ and n is a principal period for x.

Theorem 11 provides a tool for proving semiconjugacy of a map f to a subshift of finite type and thus bounding from below the topological entropy of maps by topological entropy of a shift map, which can be easily computed – see Theorem 5. It suffices to construct suitable h-sets and validate covering relations between them. In the case of the Rössler system, we managed to do this in an automatic and algorithmic way. Below, we describe the main steps of the algorithm; however, it is not possible to present all the heuristics that eventually complete the computation.

Proof of Theorem 6. Let $[a_l, a_r] \subset [a_{\min}, a_{\max}]$ be an interval of parameters. First we construct h-sets for further validation of covering relations. This computation is nonrigorous and consists of the following steps.

1. Set $a_m = \frac{1}{2}(a_l + a_r)$, $z_{\mathrm{mid}} = \frac{1}{2}(z_{\min} + z_{\max})$.
2. Find approximate extrema of $f_{a,z}$ defined in (7) for $(a,z) \in \{a_l, a_m, a_r\} \times \{z_{\min}, z_{\mathrm{mid}}, z_{\max}\}$. Observe that the number of relevant extrema of $f_{a,z}$ may depend on (a,z). Let $x_1 > \cdots > x_k$ be the approximate relevant extrema, that are present for all choices of (a,z).
3. Define $|N_i| = [x_i + \varepsilon, x_{i-1} - \varepsilon] \times [z_{\min}, z_{\max}]$ for $i = 2,\dots,k$, where $\varepsilon > 0$ is a very small number; for example, the machine epsilon $\varepsilon = 2^{-52}$.
4. From the construction, the sets $|N_i|$ are pairwise disjoint. Since x_i are approximate subsequent extrema of $f_{a,z}$, we expect $N_i \overset{P_a}{\Longrightarrow} N_j$ for all $i,j = \{2,\dots,k\}$.

5. We extend the sequence x_i by $x_0 > x_1$ and $x_{k+1} < x_k$ and define $|N_1| = [x_1 + \varepsilon, x_0] \times [z_{\min}, z_{\max}]$, $|N_{k+1}| = [x_{k+1}, x_k - \varepsilon] \times [z_{\min}, z_{\max}]$. The point x_0 is chosen so that the image $P_a(|N_1|)$ spans across as much as possible of the remaining sets $N_2, \ldots, N_k$ – see Fig. 11 and the location of B_0 and B_{odd}. This indicates that, for $a = a_{\max}$, the image $P_{a_{\max}}(|N_1|)$ spans across the sets N_i, $i = 5, \ldots, 12$. Similarly, x_{k+1} is chosen so that the image of $P_a(|N_{k+1}|)$ spans across as many as possible of sets $N_1, \ldots, N_{k+1}$. As an example, see the location of B_{13} and B_{even} in Fig. 11, which indicates that, for $a = a_{\max}$, the image $P_a(|N_{13}|)$ spans across N_i, $i = 1, \ldots, 4$.

Once h-sets N_i, $i = 1, \ldots, k+1$ have been constructed, we eventually have to rigorously compute the transition matrix of the covering relations. Observe that, from Theorem 1, the condition $P_a(|N_i|) \subset N_j^s$ from Definition 3 is always satisfied for all choice of $i, j = 1, \ldots, k+1$. Thus, to check that $N_i \overset{P_a}{\Longrightarrow} N_j$, we have to compute bounds on $P_a(N_i^{le})$ and $P_a(N_i^{re})$ and check that

- either $P_a(N_i^{re}) \subset N_j^r$ and $f(N_i^{le}) \subset N_j^l$
- or $f(N_i^{re}) \subset N_j^l$ and $f(N_i^{le}) \subset N_j^r$.

As an example, we present the data from the computation for a single parameter value $a = a_{\max}$. In the first nonrigorous step, the algorithm returns the following sequence

$$\begin{aligned}
x_0 &= -6.579089092895479, & x_1 &= -10.23628952536583,\\
x_2 &= -15.36224942593575, & x_3 &= -19.74191129794121,\\
x_4 &= -22.25394390549659, & x_5 &= -24.5784539999485,\\
x_6 &= -25.97440321955681, & x_7 &= -27.31216688246727,\\
x_8 &= -28.13292349762917, & x_9 &= -28.93522295279503,\\
x_{10} &= -29.43325241560936, & x_{11} &= -29.92639805216789,\\
x_{12} &= -30.23464037203789, & x_{13} &= -30.43604163408427,
\end{aligned} \tag{16}$$

which is used to define the h-sets N_i, $i = 1, \ldots, 13$ – see Fig. 11. Then, we compute the bounds

$$X_i := \pi_x P_{a_{\max}}\left(x_i + [-2^{-52}, 2^{-52}], [z_{\min}, z_{\max}]\right), \quad i = 0, \ldots, 13$$

and we obtain

$$\begin{aligned}
X_0 &\subset [-21.0806926149584, -21.07966553069346],\\
X_1 &\subset [-30.52865001671991, -30.52864985142989],\\
X_2 &\subset [-5.74000870675155, -5.740008372417317],\\
X_3 &\subset [-30.49586235784065, -30.49586197137184],\\
X_4 &\subset [-6.053862270340931, -6.053861581770914],\\
X_5 &\subset [-30.47672694294398, -30.47672596112965],\\
X_6 &\subset [-6.230878793151707, -6.230877235952661],\\
X_7 &\subset [-30.46181095509974, -30.46180845922029],\\
X_8 &\subset [-6.363335405504911, -6.363331754784139],\\
X_9 &\subset [-30.44856969865465, -30.44856340550682],\\
X_{10} &\subset [-6.475174472584746, -6.475165785873566],\\
X_{11} &\subset [-30.43605932780109, -30.43604364795888],\\
X_{12} &\subset [-6.575428749700791, -6.575407979118147],\\
X_{13} &\subset [-22.77372275019209, -22.75909669369429].
\end{aligned} \tag{17}$$

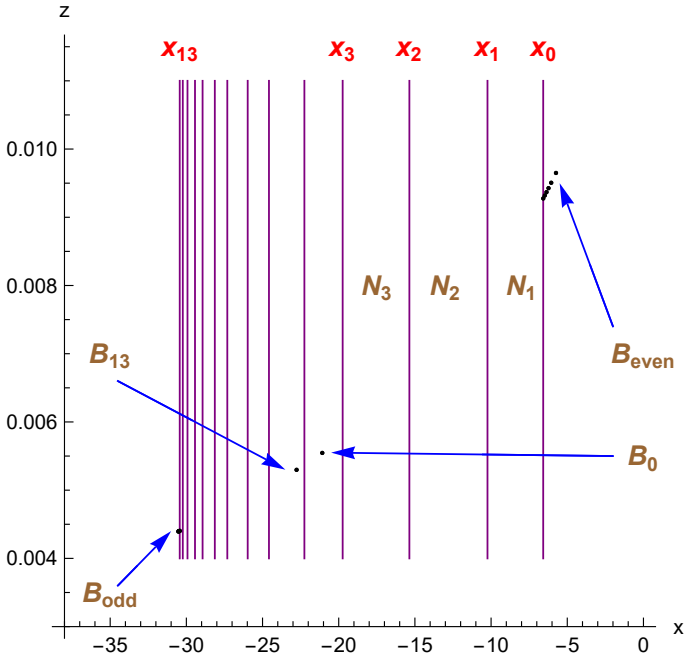

FIG. 11. Location of the edges x_i (see (16)). Rigorous tiny bounds $B_i = X_i \times Z_i = P_{a_{\max}}\left(x_i + [-2^{-52}, 2^{-52}], [z_{\min}, z_{\max}]\right), i = 0, \ldots, 13$ are marked by dots – see also (17).

The location of the line segments $\{x_i\} \times [z_{\min}, z_{\max}]$ and their corresponding bounds, $B_i = X_i \times Z_i = P_{a_{\max}}\left(x_i + [-2^{-52}, 2^{-52}], [z_{\min}, z_{\max}]\right), i = 0, \ldots, 13$, are shown in Fig. 11.

From (16) and (17), we see that

- $X_i > x_0$ for $i = 2, 4, \ldots, 12$,
- $X_i < x_{13}$ for $i = 1, 3, \ldots, 11$,
- $X_0 > x_4$ and
- $X_{13} < x_4$.

From these inequalities, we conclude that $N_i \overset{P_{a_{\max}}}{\Longrightarrow} N_j$ if $i \neq 1$, $i \neq 13$ and $j = 1, \ldots, 12$. From the bounds X_0, X_1, X_{12} and X_{13}, we also see that $N_1 \overset{P_{a_{\max}}}{\Longrightarrow} N_j$ for $j \geq 5$ and $N_{13} \overset{P_{a_{\max}}}{\Longrightarrow} N_j$ for $j = 1, \ldots, 4$. According to Theorem 11, we obtain that $P_{a_{\max}}$ restricted to $\text{Inv}\left(P_{a_{\max}}, \bigcup_{i=1}^{13} |N_i|\right)$ is semiconjugated to a shift dynamics with transition matrix M_{86} as defined in (12).

Running the above algorithm with an adaptive subdivision of the parameter range $[a_{\min}, a_{\max}]$, we obtain a semiconjugacy of P_a on the corresponding invariant set to a subshift of finite type with the topological entropy listed in Table II. □

VI. CONCLUSIONS

Topological entropy is one of the most important topological invariants in dynamical systems theory, as it is one of the possible ways to measure the complexity of the dynamics. Some landmark results by Milnor and Thurston focus on the theoretical understanding of topological entropy for

maps (discrete-time systems). We proposed an algorithmic approach to proving the existence of global changes in the topological structure of invariant sets in continuous-time systems. We applied our methodology to the classical Rössler system. For an explicit range of parameter values, we proved the existence of a trapping region that contains an attractor. By computing so-called number of relative extrema of certain Poincaré map, we showed that the topological structure of the maximal invariant set in the trapping region changes with the parameter of the system. We proved that a sequence of saddle-node bifurcations exists, giving rise to the semiconjugacy of a certain Poincaré map to symbolic dynamics in symbols from 2 to 13. This sequence of bifurcations leads to an increase in the topological entropy of the Poincaré map. The proofs of the main theorems were obtained using computer-assisted techniques.

VII. SUPPLEMENTARY MATERIAL

An integral part of this research is a C++ program that checks all inequalities related to Theorem 1, Theorem 2, Theorem 4 and Theorem 6. The source code and a description of the program is available from the public repository[54].

ACKNOWLEDGMENTS

The authors would like to thank the anonymous referees for many useful comments.

RB and SS have been supported by the Spanish Research projects PID2021-122961NB-I00 and PID2024-156032NB-I00 and the European Regional Development Fund and Diputación General de Aragón (E24-23R).

[1] J. Milnor, "On the concept of attractor," Communications in Mathematical Physics **99**, 177–195 (1985).
[2] Z. Galias, "Symbolic dynamics approach to find periodic windows: the case study of the Rössler system," Commun. Nonlinear Sci. Numer. Simul. **140**, 108403 (2025).
[3] Z. Galias, "On the density of periodic windows for the Rössler system," in *Proc. IEEE Int. Symp. Circuits Syst. (ISCAS)* (2025) pp. 1–5.
[4] D. Wilczak, S. Serrano, and R. Barrio, "Coexistence and dynamical connections between hyperchaos and chaos in the 4d Rössler system: A computer-assisted proof," SIAM Journal on Applied Dynamical Systems **15**, 356–390 (2016).
[5] O. Rössler, "An equation for continuous chaos," Physics Letters A **57**, 397–398 (1976).
[6] R. L. Adler, A. G. Konheim, and M. H. McAndrew, "Topological entropy," Transactions of the American Mathematical Society **114**, 309–319 (1965).
[7] E. Dinaburg, "A correlation between topological entropy and metric entropy," Dokl. Akad. Nauk SSSR **190**, 19–22 (1970).
[8] R. Bowen, "Entropy for group endomorphisms and homogeneous spaces," Transactions of the American Mathematical Society **153**, 401–414 (1971).
[9] A. Katok and B. Hasselblatt, *Introduction to the Modern Theory of Dynamical Systems*, Encyclopedia of Mathematics and its Applications (Cambridge University Press, 1995).
[10] J. Milnor, "Is entropy effectively computable?" Semantic Scholar (2002).
[11] S. Gangloff, A. Herrera, C. Rojas, and M. Sablik, "Computability of topological entropy: From general systems to transformations on cantor sets and the interval," Discrete and Continuous Dynamical Systems **40**, 4259–4286 (2020).
[12] R. Barrio, F. Blesa, and S. Serrano, "Qualitative analysis of the Rössler equations: Bifurcations of limit cycles and chaotic attractors," Physica D: Nonlinear Phenomena **238**, 1087–1100 (2009).
[13] R. Barrio, F. Blesa, and S. Serrano, "Unbounded dynamics in dissipative flows: Rössler model," Chaos: An Interdisciplinary Journal of Nonlinear Science **24**, 024407 (2014).
[14] R. Barrio, F. Blesa, S. Serrano, and A. Shilnikov, "Global organization of spiral structures in biparameter space of dissipative systems with Shilnikov saddle-foci," Phys. Rev. E **84**, 035201 (2011).
[15] R. Barrio, F. Blesa, and S. Serrano, "Topological changes in periodicity hubs of dissipative systems," Phys. Rev. Lett. **108**, 214102 (2012).
[16] P. Zgliczyński, "Computer assisted proof of chaos in the Rössler equations and in the Hénon map," Nonlinearity **10**, 243–252 (1997).
[17] A. Neumaier, *Interval Methods for Systems of Equations*, Encyclopedia of Mathematics and its Applications (Cambridge University Press, 1991).
[18] R. E. Moore, R. B. Kearfott, and M. J. Cloud, *Introduction to Interval Analysis* (Society for Industrial and Applied Mathematics, 2009) https://epubs.siam.org/doi/pdf/10.1137/1.9780898717716.
[19] W. Tucker, *Validated Numerics: A Short Introduction to Rigorous Computations* (Princeton University Press, USA, 2011).
[20] N. S. Nedialkov and K. R. Jackson, "An interval hermite-obreschkoff method for computing rigorous bounds on the solution of an initial value problem for an ordinary differential equation," Developments in Reliable Computing **5**, 289–310 (1998).
[21] N. Nedialkov, K. Jackson, and G. Corliss, "Validated solutions of initial value problems for ordinary differential equations," Applied Mathematics and Computation **105**, 21 – 68 (1999).
[22] N. S. Nedialkov, K. R. Jackson, and J. D. Pryce, "An effective high-order interval method for validating existence and uniqueness of the solution of an ivp for an ode," Reliable Computing **7**, 449–465 (2001).
[23] N. S. Nedialkov, "Vnode-lp: A validated solver for initial value problems in ordinary differential equations," Tech. Rep. Technical Report CAS-06-06-NN (McMaster University, Canada, 2006).
[24] A. Rauh, M. Brill, and C. GüNther, "A novel interval arithmetic approach for solving differential-algebraic equations with ValEncIA-IVP," Int. J. Appl. Math. Comput. Sci. **19**, 381–397 (2009).
[25] T. Kapela, M. Mrozek, D. Wilczak, and P. Zgliczyński, "CAPD::DynSys: A flexible C++ toolbox for rigorous numerical analysis of dynamical systems," Communications in Nonlinear Science and Numerical Simulation **101**, 105578 (2021).
[26] P. Zgliczyński, "$\mathscr{C}^1$-Lohner algorithm," Foundations of Computational Mathematics **2**, 429–465 (2002).
[27] I. Walawska and D. Wilczak, "An implicit algorithm for validated enclosures of the solutions to variational equations for ODEs," Applied Mathematics and Computation **291**, 303–322 (2016).
[28] D. Wilczak and P. Zgliczyński, "$\mathscr{C}^r$-Lohner algorithm," Schedae Informaticae **20**, 9–46 (2011).
[29] T. Kapela, D. Wilczak, and P. Zgliczyński, "Recent advances in a rigorous computation of Poincaré maps," Communications in Nonlinear Science and Numerical Simulation **110**, 106366 (2022).
[30] M. J. Capiński, J. D. Mireles James, W. Tucker, D. Wilczak, and J. B. van den Berg, "Computer assisted proofs in dynamical systems," Communications in Nonlinear Science and Numerical Simulation **118**, 106998 (2023).
[31] M. J. Capiński, E. Fleurantin, and J. D. M. James, "Computer assisted proofs of two-dimensional attracting invariant tori for ODEs," Discrete and Continuous Dynamical Systems - A **40**, 6681 (2020).
[32] F. A. Bartha and W. Tucker, "Fixed points of a destabilized Kuramoto–Sivashinsky equation," Applied Mathematics and Computation **266**, 339 – 349 (2015).
[33] M. J. Capiński, "Computer assisted existence proofs of Lyapunov orbits at L2 and transversal intersections of invariant manifolds in the Jupiter-Sun PCR3BP," SIAM J. Applied Dynamical Systems **11**, 1723–1753 (2012).
[34] J. Cyranka and T. Wanner, "Computer-assisted proof of heteroclinic connections in the one-dimensional Ohta–Kawasaki model," SIAM Journal on Applied Dynamical Systems **17**, 694–731 (2018).
[35] J. Galante and V. Kaloshin, "Destruction of invariant curves in the restricted circular planar three body problem using comparison of action," Duke Math. J. **159**, 275–327 (2011).
[36] M. Cadiot, J.-P. Lessard, and J.-C. Nave, "Rigorous computation of solutions of semilinear pdes on unbounded domains via spectral methods,"

SIAM Journal on Applied Dynamical Systems **23**, 1966–2017 (2024).
[37] J.-P. L. Gabriel William Duchesne and A. Takayasu, "A rigorous integrator and global existence for higher-dimensional semilinear parabolic pdes via semigroup theory," Journal of Scientific Computing **62** (2025), https://doi.org/10.1007/s10915-024-02785-x.
[38] R. Barrio, M. Rodríguez, and F. Blesa, "Computer-assisted proof of skeletons of periodic orbits," Computer Physics Communications **183**, 80–85 (2012).
[39] W. Tucker, "A rigorous ODE solver and Smale's 14th problem," Found. Comput. Math. **2**, 53–117 (2002).
[40] P. Góra and A. Boyarsky, "Computing the topological entropy of general one-dimensional maps," Transactions of the American Mathematical Society **323**, 39–49 (1991).
[41] J. Milnor and W. Thurston, "On iterated maps of the interval," in *Dynamical Systems*, edited by J. C. Alexander (Springer Berlin Heidelberg, Berlin, Heidelberg, 1988) pp. 465–563.
[42] A. Wolf, J. B. Swift, H. L. Swinney, and J. A. Vastano, "Determining Lyapunov exponents from a time series," Physica D: Nonlinear Phenomena **16**, 285–317 (1985).
[43] E. Doedel, "AUTO: a program for the automatic bifurcation analysis of autonomous systems," Congr. Numer. **30**, 265–284 (1981).
[44] E. J. Doedel, R. Paffenroth, A. R. Champneys, T. F. Fairgrieve, Y. A. Kuznetsov, B. E. Oldeman, B. Sandstede, and X. J. Wang, "Auto2000," `http://cmvl.cs.concordia.ca/auto` (2000).
[45] J. S. Birman and R. Williams, "Knotted periodic orbits in dynamical systems—i: Lorenz's equation," Topology **22**, 47–82 (1983).
[46] C. Letellier, P. Dutertre, and B. Maheu, "Unstable periodic orbits and templates of the Rössler system: Toward a systematic topological characterization," Chaos: An Interdisciplinary Journal of Nonlinear Science **5**, 271–282 (1995).
[47] G. Boulant, M. Lefranc, S. Bielawski, and D. Derozier, "A nonhorseshoe template in a chaotic laser model," International Journal of Bifurcation and Chaos **08**, 965–975 (1998).
[48] J. Used and J. C. Martín, "Multiple topological structures of chaotic attractors ruling the emission of a driven laser," Phys. Rev. E **82**, 016218 (2010).
[49] S. Serrano, M. A. Martínez, and R. Barrio, "Order in chaos: Structure of chaotic invariant sets of square-wave neuron models," Chaos: An Interdisciplinary Journal of Nonlinear Science **31**, 043108 (2021).
[50] R. Gilmore, "Topological analysis of chaotic dynamical systems," Rev. Mod. Phys. **70**, 1455–1529 (1998).
[51] R. Gilmore and M. Lefranc, *The topology of chaos* (Wiley-Interscience [John Wiley & Sons], New York, 2002).
[52] H. Kantz and P. Grassberger, "Repellers, semi-attractors, and long-lived chaotic transients," Physica D: Nonlinear Phenomena **17**, 75–86 (1985).
[53] J. Guckenheimer and P. Holmes, *Nonlinear Oscillations, Dynamical Systems, and Bifurcations of Vector Fields* (Springer, Berlin, 1983).
[54] D. Wilczak, "Supplementary material – repository of the C++ source code," `https://github.com/dbwilczak/entropy-growth` (2025).
[55] I. Walawska and D. Wilczak, "Validated numerics for period-tupling and touch-and-go bifurcations of symmetric periodic orbits in reversible systems," Communications in Nonlinear Science and Numerical Simulation **74**, 30 – 54 (2019).
[56] P. Zgliczyński and M. Gidea, "Covering relations for multidimensional dynamical systems," Journal of Differential Equations **202**, 32–58 (2004).
[57] R. W. Easton, "Isolating blocks and symbolic dynamics," Journal of Differential Equations **17**, 96–118 (1975).